Electronic Supplementary Information

A fluorescent methylation-switchable probe for highly sensitive analysis of FTO N^6-methyladenosine demethylase activity in cells†

Adeline Cheong,[a] Joanne J. A. Low,[a] Andrea Lim,[a,b] Paul M. Yen,[b] and Esther C. Y. Woon[*,a]

[a]Department of Pharmacy, National University of Singapore, 18 Science Drive 4, 117543, Singapore.

[b]Program of Cardiovascular and Metabolic Disorders, Duke-NUS Medical School, 8 College Road, 169857, Singapore

* To whom correspondence should be addressed.

Esther C. Y. Woon

Email: esther.woon@nus.edu.sg Fax: Tel: (+65) 6516 2932; (+65) 6779 1554.

Contents:

Materials and methods

Table S1. Sequences of 2'-*O*-Me RNA probes investigated in this study and their MALDI-TOF MS data.

	Probe	Sequence	MALDI-MS	
			$[M+H]^+$ (calculated)	$[M+H]^+$ (observed)
14mer	**1a**	2'-OMe(GCGCG A^{m6}GCU CGCGC)	4687.1	4687.9
	1b	2'-OMe(GCGCG AGCU CGCGC)	4673.3	4673.3
12mer	**2a**	2'-OMe(GCCG A^{m6}GCU CGGC)	4008.8	4008.6
	2b	2'-OMe(GCCG AGCU CGGC)	3994.7	3994.9
	3a	2'-OMe(CGCG A^{m6}GCU CGCG)	4008.5	4008.5
	3b	2'-OMe(CGCG AGCU CGCG)	3994.1	3994.4
	4a	2'-OMe(CGGC A^{m6}GCU GCCG)	4008.9	4008.7
	4b	2'-OMe(CGGC AGCU GCCG)	3994.2	3994.8
	5a	2'-OMe(CCGG A^{m6}GCU CCGG)	4008.8	4008.5
	5b	2'-OMe(CCGG AGCU CCGG)	3994.7	3994.8
10mer	**6a**	2'-OMe(GCC A^{m6}GCU GGC)	3330.3	3330.0
	6b	2'-OMe(GCC AGCU GGC)	3316.2	3316.9
	7a	2'-OMe(GCG A^{m6}GCU CGC)	3330.2	3330.3
	7b	2'-OMe(GCG AGCU CGC)	3316.5	3316.4
	8a	2'-OMe(GGC A^{m6}GCU GCC)	3330.2	3330.2
	8b	2'-OMe(GGC AGCU GCC)	3316.0	3316.1
	9a	2'-OMe(CCG A^{m6}GCU CGG)	3330.3	3330.0
	9b	2'-OMe(CCG AGCU CGG)	3316.1	3316.9
	10a	2'-OMe(CGG A^{m6}GCU CCG)	3330.4	3330.1
	10b	2'-OMe(CGG AGCU CCG)	3316.2	3316.1
Analogues of **8**	**11a**	2'-OMe(GGC A^{m6}GUACU GCC)	3993.6	3993.6
	11b	2'-OMe(GGC AGUACU GCC)	3979.5	3979.5
	12a	2'-OMe(GGC A^{m6}GAUCU GCC)	3993.2	3993.8
	12b	2'-OMe(GGC AGAUCU GCC)	3979.7	3979.6

Table S2. Sequences of fluorescent probes investigated in this study and their MALDI-TOF MS data. The fluorescent reporter, 2′-*O*-(1-pyrenylmethyl)uridine (U^p), contains a pyrene fluorophore tethered to the 2'-*O*-position of uridine *via* a methylene linkage.

	Probe	Sequence	MALDI-MS	
			$[M+H]^+$ (calculated)	$[M+H]^+$ (observed)
Analogues of probe **8**	**13a**	2'-OMe(GGC A^{m6}GCU^p GCC)	3532.3	3532.4
	13b	2'-OMe(GGC AGCU^p GCC)	3518.2	3518.5
Analogues of probe **11**	**14a**	2'-OMe(GGC A^{m6}GU^pACU GCC)	4195.4	4195.5
	14b	2'-OMe(GGC AGU^pACU GCC)	4181.6	4181.3
	15a	2'-OMe(GGC A^{m6}GUACU^p GCC)	4195.5	4195.9
	15b	2'-OMe(GGC AGUACU^p GCC)	4181.4	4181.1
Analogues of probe **12**	**16a**	2'-OMe(GGC A^{m6}GAU^pCU GCC)	4195.1	4195.4
	16b	2'-OMe(GGC AGAU^pCU GCC)	4181.7	4181.2
	17a	2'-OMe(GGC A^{m6}GAUCU^p GCC)	4195.1	4195.5
	17b	2'-OMe(GGC AGAUCU^p GCC)	4181.4	4181.7
	18a (m^6A-probe)	2'-OMe(GGC A^{m6}GAU^pCU^p GCC)	4397.7	4397.3
	18b	2'-OMe(GGC AGAU^pCU^p GCC)	4383.5	4383.6
	19a (control probe)	2'-OMe(GGC A^{m6}GCU^pCU^p GCC)	4373.2	4373.5
	19b	2'-OMe(GGC AGCU^pCU^p GCC)	4359.6	4359.8
	20a (m^1A-probe)	2'-OMe(GGC A^{m1}GAU^pCU^p GCC)	4397.7	4397.4
	20b	2'-OMe(GGC AGAU^pCU^p GCC)	4383.7	4383.6
	21a (m^1G-probe)	2'-OMe(GGC AG^{m1}AU^pCU^p GCC)	4397.4	4397.8
	21b	2'-OMe(GGC AGAU^pCU^p GCC)	4383.3	4383.5
	22a (m^3dC-probe)	2'-OMe(GGC AGAU^p dC^{m3} U^p GCC)	4367.2	4367.1
	22b	2'-OMe(GGC AGAU^p dC U^p GCC)	4353.1	4353.5

a.

Total strand conc/ μM	T_m/°C	
	1a	1b
50	91.7	94.2
30	90.2	93.4
20	89.9	92.5
10	89.4	92.0
5	87.6	90.5
2	85.8	88.8
1	84.0	87.7

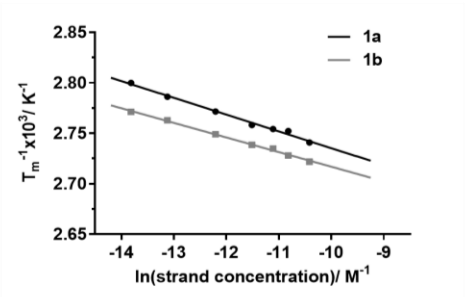

Probe	Sequence	Preferred conformation	T_m (°C) (at 5 μM)[a]	$\Delta H°$ (kcal/mol)[b]	$\Delta S°$ (cal/mol/K)[b]	$\Delta G°_{310}$ (kcal/mol)
1a	2'-OMe(GCGCG m^6AGCU CGCGC)	Duplex	87.6 ± 0.3	-125.0 ± 1.5	-322.2 ± 1.9	-25.1 ± 0.1
1b	2'-OMe(GCGCG AGCU CGCGC)	Duplex	90.5 ± 0.3	-131.3 ± 1.5	-336.7 ± 2.5	-26.9 ± 0.1

b.

Total strand conc/ μM	T_m/°C	
	2a	2b
50	79.3	82.2
30	78.4	81.2
20	77.6	80.8
10	76.7	80.1
5	75.4	78.4
2	73.7	76.3
1	72.2	75.3

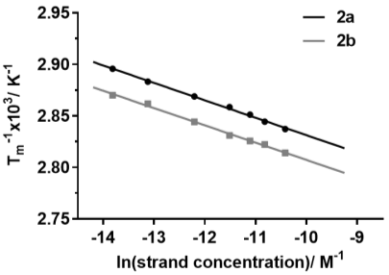

Probe	Sequence	Preferred conformation	T_m (°C) (at 5 μM)[a]	$\Delta H°$ (kcal/mol)[b]	$\Delta S°$ (cal/mol/K)[b]	$\Delta G°_{310}$ (kcal/mol)
2a	2'-OMe(GCCG m^6AGCU CGGC)	Duplex	75.4 ± 0.2	-112.3 ± 0.8	-297.9 ± 2.1	-20.0 ± 0.2
2b	2'-OMe(GCCG AGCU CGGC)	Duplex	78.4 ± 0.5	-117.7 ± 1.0	-310.5 ± 3.0	-21.5 ± 0.2

Fig. S1. UV-based melting analysis of m^{6}A-containing probes and their non-methylated counterparts. (a) The UV melting transitions of the methylated probe **1a** (black line) and non-methylated probe **1b** (grey line) were measured at total strand concentrations between 1-50 μM under physiologically-relevant conditions (10 mM sodium phosphate buffer containing 150 mM NaCl, pH 7.4). Van't Hoff analysis of **1a** and **1b** revealed concentration-dependent T_ms, implying that both probes exist predominantly as bimolecular duplex structures under our experimental conditions. The thermodynamic data were derived from $1/T_m$ versus ln(strand concentration) plot, assuming a two-state process. (b) The UV melting and thermodynamic analyses of **2a** (black line) and **2b** (grey line) were determined as described above. Both probes again exhibited concentration-dependent T_ms, implying that they exist predominantly as bimolecular duplex structures under our experimental conditions.

a.

Total strand conc/ μM	T_m/ °C	
	3a	3b
50	77.5	79.0
30	76.7	78.1
20	75.7	77.5
10	75.0	76.9
5	73.5	75.1
2	71.5	73.5
1	70.0	71.4

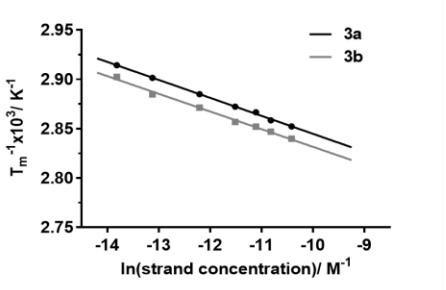

Probe	Sequence	Preferred conformation	T_m (°C) (at 5 μM)[a]	$\Delta H°$ (kcal/mol)[b]	$\Delta S°$ (cal/mol/K)[b]	$\Delta G°_{310}$ (kcal/mol)
3a	2'-OMe(CGCG m^6AGCU CGCG)	Duplex	73.5 ± 0.5	-109.0 ± 0.7	-290.2 ± 2.5	-19.2 ± 0.2
3b	2'-OMe(CGCG AGCU CGCG)	Duplex	75.1 ± 0.3	-113.2 ± 1.2	-300.2 ± 3.4	-20.0 ± 0.1

b.

Total strand conc/ μM	T_m/ °C	
	4a	4b
50	81.5	84.3
30	80.3	83.1
20	80.0	82.5
10	78.9	81.4
5	77.4	80.2
2	75.5	78.0
1	74.4	76.9

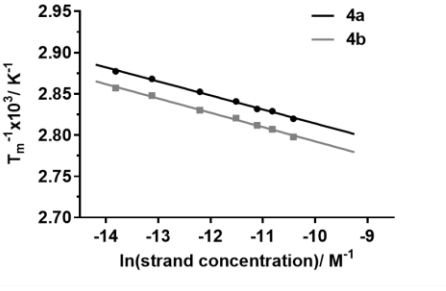

Probe	Sequence	Preferred conformation	T_m (°C) (at 5 μM)[a]	$\Delta H°$ (kcal/mol)[b]	$\Delta S°$ (cal/mol/K)[b]	$\Delta G°_{310}$ (kcal/mol)
4a	2'-OMe(CGGC m^6AGCU GCCG)	Duplex	77.4 ± 0.3	-116.9 ± 0.5	-309.2 ± 2.0	-21.2 ± 0.1
4b	2'-OMe(CGGC AGCU GCCG)	Duplex	80.2 ± 0.2	-119.1 ± 0.9	-312.8 ± 3.6	-22.1 ± 0.1

Fig. S2. UV-based melting analysis of m^6A-containing probes and their non-methylated counterparts. (a) The UV melting transitions of the methylated probe **3a** (black line) and non-methylated probe **3b** (grey line) were measured at total strand concentrations between 1-50 μM under physiologically-relevant conditions (10 mM sodium phosphate buffer containing 150 mM NaCl, pH 7.4). Van't Hoff analysis of **3a** and **3b** revealed concentration-dependent T_ms, implying that both probes exist predominantly as bimolecular duplex structures under our experimental conditions. The thermodynamic data were derived from $1/T_m$ versus ln(strand concentration) plot, assuming a two-state process. (b) The UV melting and thermodynamic analyses of **4a** (black line) and **4b** (grey line) were determined as described above. Both probes again exhibited concentration-dependent T_m, implying that they exist predominantly as bimolecular duplex structures under our experimental conditions.

a.

Total strand conc/ μM	T_m/°C	
	5a	5b
50	77.5	80.3
30	76.9	79.4
20	76.3	78.5
10	75.7	77.6
5	73.8	76.5
2	71.8	74.6
1	70.0	73.5

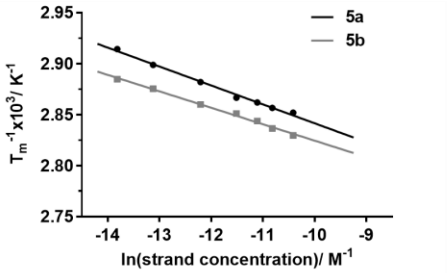

Probe	Sequence	Preferred conformation	T_m (°C) (at 5 μM)[a]	$\Delta H°$ (kcal/mol)[b]	$\Delta S°$ (cal/mol/K)[b]	$\Delta G°_{310}$ (kcal/mol)
5a	2'-OMe(CCGG m^6AGCU CCGG)	Duplex	73.8 ± 0.4	-108.8 ± 1.1	-289.3 ± 2.7	-19.1 ± 0.2
5b	2'-OMe(CCGG AGCU CCGG)	Duplex	76.5 ± 0.5	-117.4 ± 1.0	-311.5 ± 3.1	-20.8 ± 0.2

b.

Total strand conc/ μM	T_m/°C	
	6a	6b
50	68.4	70.5
30	67.4	69.3
20	66.8	68.7
10	65.9	67.2
5	63.8	65.6
2	61.6	63.3
1	59.6	61.3

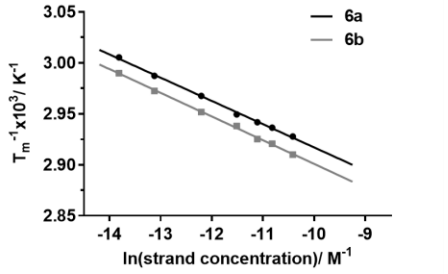

Probe	Sequence	Preferred conformation	T_m (°C) (at 5 μM)[a]	$\Delta H°$ (kcal/mol)[b]	$\Delta S°$ (cal/mol/K)[b]	$\Delta G°_{310}$ (kcal/mol)
6a	2'-OMe(GCC m^6AGCU GGC)	Duplex	63.8 ± 0.4	-84.7 ± 1.5	-227.1 ± 2.1	-14.3 ± 0.1
6b	2'-OMe(GCC AGCU GGC)	Duplex	65.6 ± 0.5	-88.1 ± 1.0	-235.8 ± 2.4	-15.0 ± 0.2

Fig. S3. UV-based melting analysis of m^{6}A-containing probes and their non-methylated counterparts. (a) The UV melting transitions of the methylated probe **5a** (black line) and non-methylated probe **5b** (grey line) were measured at total strand concentrations between 1-50 μM under physiologically-relevant conditions (10 mM sodium phosphate buffer containing 150 mM NaCl, pH 7.4). Van't Hoff analysis of **5a** and **5b** revealed concentration-dependent T_ms, implying that both probes exist predominantly as bimolecular duplex structures under our experimental conditions. The thermodynamic data were derived from $1/T_m$ versus ln(strand concentration) plot, assuming a two-state process. (b) The UV melting and thermodynamic analyses of **6a** (black line) and **6b** (grey line) were determined as described above. Both probes again exhibited concentration-dependent T_m, implying that they exist predominantly as bimolecular duplex structures under our experimental conditions.

a.

Total strand conc/ μM	T_m/°C	
	7a	7b
50	68.1	69.2
30	67.0	67.9
20	66.5	67.4
10	65.1	66.0
5	63.6	64.2
2	61.1	61.6
1	59.3	60.4

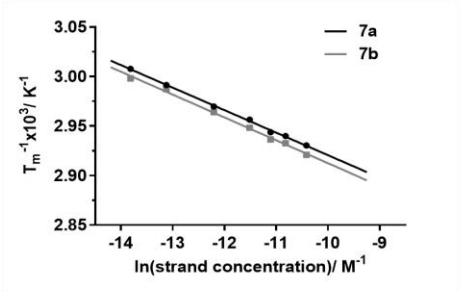

Probe	Sequence	Preferred conformation	T_m (°C) (at 5 μM)[a]	$\Delta H°$ (kcal/mol)[b]	$\Delta S°$ (cal/mol/K)[b]	$\Delta G°_{310}$ (kcal/mol)
7a	2'-OMe(GCG A^{m6}GCU CGC)	Duplex	63.6 ± 0.2	-84.1 ± 1.3	-225.5 ± 3.4	-14.2 ± 0.1
7b	2'-OMe(GCG AGCU CGC)	Duplex	64.2 ± 0.3	-87.4 ± 0.4	-234.8 ± 1.9	-14.6 ± 0.1

b.

Total strand conc/ μM	T_m/°C	
	8a	8b
50	69.5	69.9
30	69.2	68.8
20	68.9	68.3
10	69.2	67.1
5	69.2	65.3
2	69.0	62.8
1	69.4	61.4

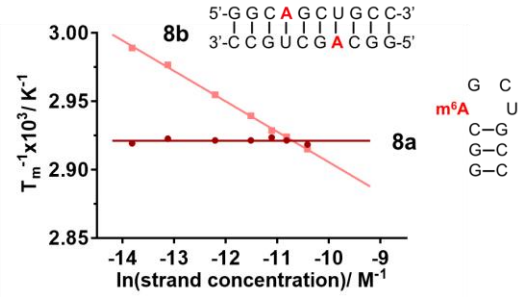

Probe	Sequence	Preferred conformation	T_m (°C) (at 5 μM)[a]	$\Delta H°$ (kcal/mol)[b]	$\Delta S°$ (cal/mol/K)[b]	$\Delta G°_{310}$ (kcal/mol)
8a	2'-OMe(GGC A^{m6}GCU GCC)	Hairpin	69.2 ± 0.5	-36.9 ± 1.5	-107.8 ± 3.6	-3.5 ± 0.2
8b	2'-OMe(GGC AGCU GCC)	Duplex	65.3 ± 0.5	-89.5 ± 0.7	-240.2 ± 2.1	-15.0 ± 0.2

Fig. S4. UV-based melting analysis of m^{6}A-containing probes and their non-methylated counterparts. (a) The UV melting transitions of the methylated probe **7a** (black line) and non-methylated probe **7b** (grey line) were measured at total strand concentrations between 1-50 μM under physiologically-relevant conditions (10 mM sodium phosphate buffer containing 150 mM NaCl, pH 7.4). Van't Hoff analysis of **7a** and **7b** revealed concentration-dependent T_ms, implying that both probes exist predominantly as bimolecular duplex structures under our experimental conditions. The thermodynamic data were derived from $1/T_m$ versus ln(strand concentration) plot, assuming a two-state process. (b) The UV melting profiles of methylated probe **8a** (red line) and non-methylated probe **8b** (pink line) were determined as described above. Whereas **8a** showed a concentration-independent T_m, which is characteristic of a monomolecular hairpin structure, its non-methylated equivalent **8b** exhibited a concentration-dependent T_m, implying a bimolecular duplex structure. The thermodynamic data of **8a** was obtained from α (the fraction of strands remaining hybridised) versus temperature plot by curve fitting to a two-state transition model, whilst that of **8b** was derived from $1/T_m$ versus ln(strand concentration) plot, assuming a two-state process.

a.

Total strand conc/ μM	T_m/°C	
	9a	9b
50	65.7	68.4
30	64.8	67.1
20	64.2	66.5
10	62.9	65.1
5	60.9	63.2
2	58.6	60.6
1	56.4	58.7

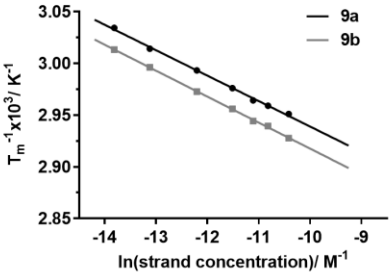

Probe	Sequence	Preferred conformation	T_m (°C) (at 5 μM)[a]	$\Delta H°$ (kcal/mol)[b]	$\Delta S°$ (cal/mol/K)[b]	$\Delta G°_{310}$ (kcal/mol)
9a	2'-OMe(CCG m^6AGCU CGG)	Duplex	60.9 ± 0.4	-80.5 ± 0.8	-216.7 ± 2.8	-13.3 ± 0.1
9b	2'-OMe(CCG AGCU CGG)	Duplex	63.2 ± 0.2	-82.4 ± 0.9	-220.7 ± 2.1	-14.0 ± 0.2

b.

Total strand conc/ μM	T_m/°C	
	10a	10b
50	66.8	70.1
30	65.2	69.0
20	64.7	68.4
10	63.8	67.6
5	61.7	65.5
2	59.1	63.2
1	57.5	61.6

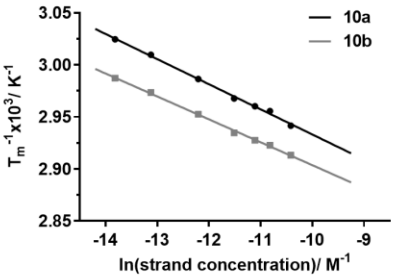

Probe	Sequence	Preferred conformation	T_m (°C) (at 5 μM)[a]	$\Delta H°$ (kcal/mol)[b]	$\Delta S°$ (cal/mol/K)[b]	$\Delta G°_{310}$ (kcal/mol)
10a	2'-OMe(CGG m^6AGCU CCG)	Duplex	61.7 ± 0.5	-83.8 ± 1.2	-226.0 ± 3.4	-13.7 ± 0.1
10b	2'-OMe(CGG AGCU CCG)	Duplex	65.5 ± 0.2	-87.4 ± 1.0	-233.8 ± 2.5	-14.9 ± 0.1

Fig. S5. UV-based melting analysis of m^6A-containing probes and their non-methylated counterparts. (a) The UV melting transitions of the methylated probe **9a** (black line) and non-methylated probe **9b** (grey line) were measured at total strand concentrations between 1-50 μM under physiologically-relevant conditions (10 mM sodium phosphate buffer containing 150 mM NaCl, pH 7.4). Van't Hoff analysis of **9a** and **9b** revealed concentration-dependent T_ms, implying that both probes exist predominantly as bimolecular duplex structures under our experimental conditions. The thermodynamic data were derived from $1/T_m$ versus ln(strand concentration) plot, assuming a two-state process. (b) The UV melting and thermodynamic analyses of **10a** (black line) and **10b** (grey line) were determined as described above. Both probes again exhibited concentration-dependent T_m, implying that they exist predominantly as bimolecular duplex structures under our experimental conditions.

a.

Total strand conc/ μM	T_m/°C	
	11a	11b
50	73.4	72.2
30	73.1	70.8
20	73.3	70.4
10	72.9	69.2
5	73.1	67.8
2	73.1	65.5
1	72.8	64.3

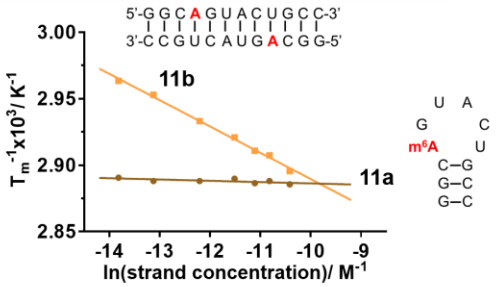

Probe	Sequence	Preferred conformation	T_m (°C) (at 5 μM)[a]	ΔH° (kcal/mol)[b]	ΔS° (cal/mol/K)[b]	ΔG°_{310} (kcal/mol)
11a	2'-OMe(GGC A^{m6}GUACU GCC)	Hairpin	73.1 ± 0.2	-42.0 ± 0.6	-121.3 ± 2.7	-4.4 ± 0.1
11b	2'-OMe(GGC AGUACU GCC)	Duplex	67.8 ± 0.3	-99.4 ± 1.1	-267.3 ± 3.5	-16.5 ± 0.1

b.

Total strand conc/ μM	T_m/°C	
	12a	12b
50	73.8	71.7
30	73.3	70.5
20	73.5	69.6
10	73.7	68.7
5	73.5	67.3
2	73.5	64.9
1	73.2	63.7

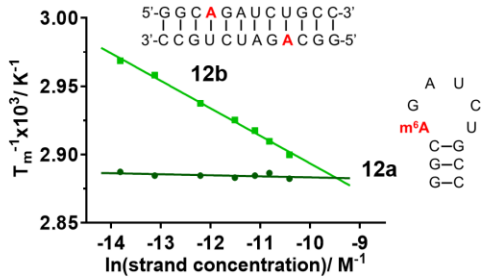

Probe	Sequence	Preferred conformation	T_m (°C) (at 5 μM)[a]	ΔH° (kcal/mol)[b]	ΔS° (cal/mol/K)[b]	ΔG°_{310} (kcal/mol)
12a	2'-OMe(GGC A^{m6}GAUCU GCC)	Hairpin	73.5 ± 0.4	-41.6 ± 0.7	-120.0 ± 1.7	-4.4 ± 0.2
12b	2'-OMe(GGC AGAUCU GCC)	Duplex	67.3 ± 0.3	-98.5 ± 1.4	-265.1 ± 3.1	-16.3 ± 0.1

Fig. S6. UV-based melting analysis of m^6A-containing probes and their non-methylated counterparts. (a) The UV melting transitions of the methylated probe **11a** (brown line) and non-methylated probe **11b** (orange line) were measured at total strand concentrations between 1-50 μM under physiologically-relevant conditions (10 mM sodium phosphate buffer containing 150 mM NaCl, pH 7.4). Van't Hoff analysis of **11a** revealed a concentration-independent T_m, which is characteristic of a monomolecular hairpin structure. Its non-methylated equivalent **11b** exhibited a concentration-dependent T_m, implying a bimolecular duplex structure. The thermodynamic data of **11a** was obtained from α (the fraction of strands remaining hybridised) versus temperature plot by curve fitting to a two-state transition model, whilst that of **11b** was derived from $1/T_m$ versus ln(strand concentration) plot, assuming a two-state process. (b) The UV melting and thermodynamic analyses of methylated probe **12a** (green line) and non-methylated probe **12b** (pale green line) were determined as described above. Whereas **12a** showed a concentration-independent T_m, which is characteristic of a monomolecular hairpin structure, its non-methylated equivalent **12b** exhibited a concentration-dependent T_m, implying a bimolecular duplex structure.

a.

Total strand conc/ μM	T_m/°C	
	18a	18b
50	72.2	69.4
30	72.5	68.2
20	72.0	68.0
10	72.2	66.8
5	72.2	65.2
2	72.4	62.8
1	71.9	61.5

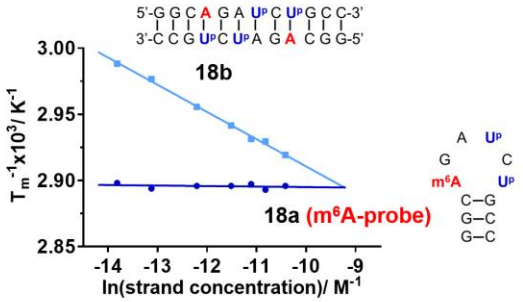

Probe	Sequence	Preferred conformation	T_m (°C) (at 5 μM)[a]	$\Delta H°$ (kcal/mol)[b]	$\Delta S°$ (cal/mol/K)[b]	$\Delta G°_{310}$ (kcal/mol)
18a (m^{6}A-probe)	2'-OMe(GGC ^{m6}AGAU^{P}CU^P GCC)	Hairpin	72.2 ± 0.5	-42.3 ± 1.3	-122.5 ± 2.5	-4.3 ± 0.2
18b (Demethylated probe)	2'-OMe(GGC AGAU^{P}CU^P GCC)	Duplex	65.2 ± 0.4	-97.9 ± 0.5	-265.2 ± 3.8	-15.7 ± 0.2

b.

Total strand conc/ μM	T_m/°C	
	19a	19b
50	71.3	71.5
30	71.0	71.9
20	71.6	71.6
10	71.5	71.5
5	71.4	71.8
2	71.2	71.3
1	71.9	71.0

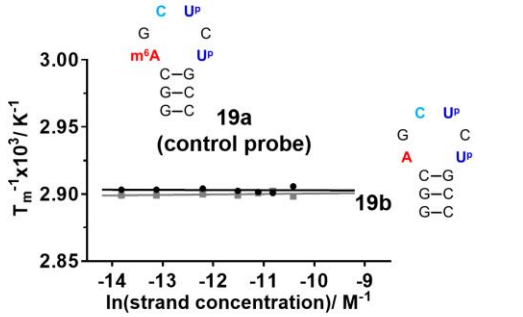

Probe	Sequence	Preferred conformation	T_m (°C) (at 5 μM)[a]	$\Delta H°$ (kcal/mol)[b]	$\Delta S°$ (cal/mol/K)[b]	$\Delta G°_{310}$ (kcal/mol)
19a (control probe)	2'-OMe(GGC ^{m6}AGCU^{P}CU^P GCC)	Hairpin	71.4 ± 0.8	-40.5 ± 1.5	-117.3 ± 1.3	-4.1 ± 0.2
19b	2'-OMe(GGC AGCU^{P}CU^P GCC)	Hairpin	71.8 ± 0.3	-41.2 ± 1.7	-119.4 ± 2.4	-4.2 ± 0.2

Fig. S7. UV-based melting analysis of m^{6}A-containing probes and their non-methylated counterparts. (a) The UV melting transitions of the methylated probe **18a** (**m^{6}A-probe**; blue line) and non-methylated probe **18b** (pale blue line) were measured at total strand concentrations between 1-50 μM under physiologically-relevant conditions (10 mM sodium phosphate buffer containing 150 mM NaCl, pH 7.4). Van't Hoff analysis of **18a** revealed a concentration-independent T_m, which is characteristic of a monomolecular hairpin structure. Its non-methylated equivalent **18b** exhibited a concentration-dependent T_m, implying a bimolecular duplex structure. The thermodynamic data of **18a** was obtained from α (the fraction of strands remaining hybridised) versus temperature plot by curve fitting to a two-state transition model, whilst that of **18b** was derived from $1/T_m$ versus ln(strand concentration) plot, assuming a two-state process. (b) The UV melting profiles of the non-palindromic control probe **19a** (black line) and its non-methylated counterpart **19b** (grey line) were determined as described above. Both probes exhibited concentration-independent T_m, implying that they exist predominantly as monomolecular hairpin structures under our experimental conditions. The thermodynamic data of **19a** and **19b** were obtained from α (the fraction of strands remaining hybridised) versus temperature plot by curve fitting to a two-state transition model.

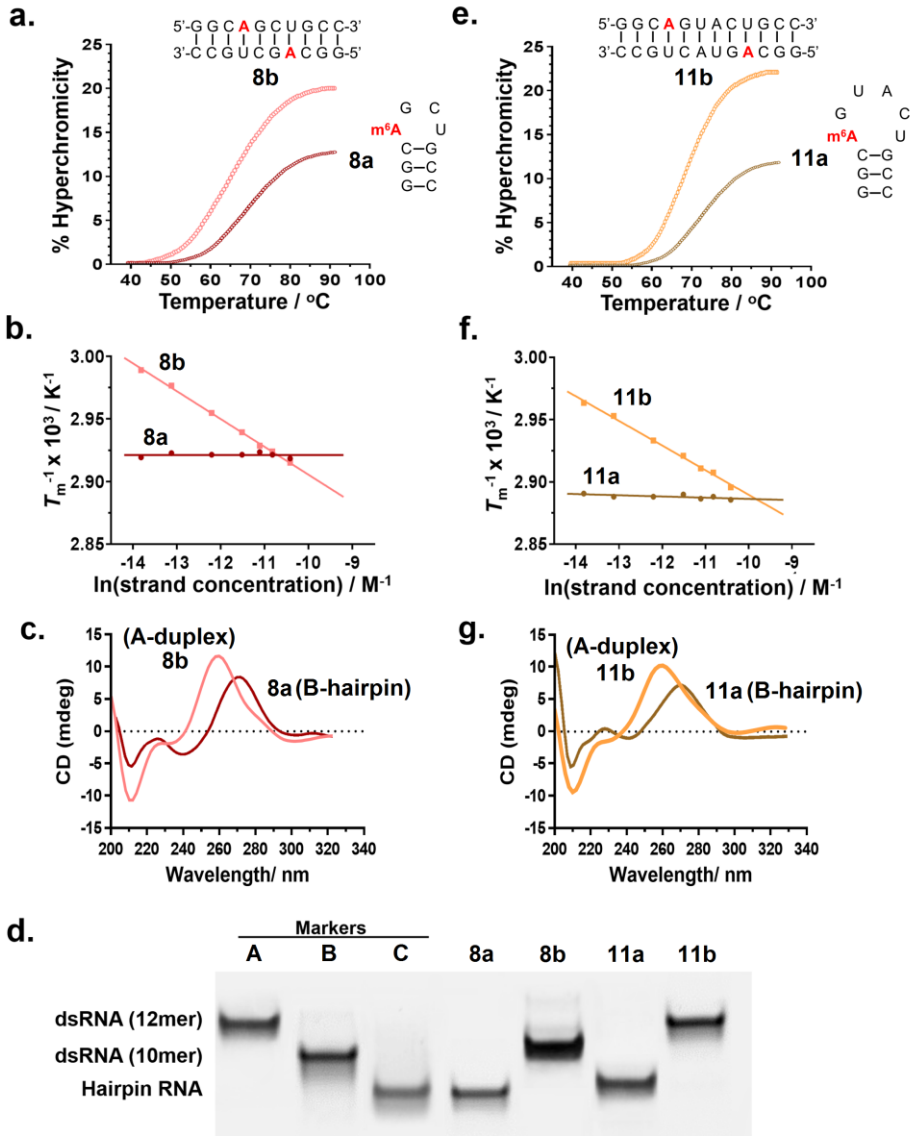

Fig. S8. Conformational analyses of probes **8a** and **11a**. (a) Overlay of the UV melting profiles of methylated probes **8a** (red line) and its non-methylated counterparts **8b** (pink line), both measured at 5 µM total strand concentrations in 10 mM sodium phosphate buffer containing 150 mM NaCl, pH 7.0. The melt profile revealed a monophasic, sigmoid melt transition, implying that both probes exist predominantly as single conformation under our experimental conditions. (b) Van't Hoff analysis of **8a** revealed a concentration-independent T_m, which is characteristic of a monomolecular hairpin structure. Its non-methylated equivalent **8b** exhibited a concentration dependent T_m, implying a bimolecular duplex structure. The thermodynamic data of **8a** was obtained from α (the fraction of strands remaining hybridised) versus temperature plot by curve fitting to a two-state transition model, whilst that of **8b** was derived from $1/T_m$ versus ln(strand concentration) plot, assuming a two-state process. (c) CD analysis (at 5 µM strand concentration) revealed a B-like hairpin structure for **8a** and an A-form duplex

for **8b**. (d) Native polyacrylamide gel electrophoresis showed only one discrete band for each strand, suggesting that they exist exclusively as hairpin or duplex structure, rather than a mixture of conformations. The methylated probes **11a** (brown line) and its non-methylated counterparts **11b** (orange line) were also found to exist predominantly as hairpin and duplex conformations, respectively, as demonstrated by (d) native gel electrophoresis, (e) UV-based melting analysis, (f) van't Hoff plots, and (g) CD spectroscopy. Marker A: 12mer dsRNA r(CGCGCGCGCGCG)^2; marker B: 10mer dsRNA r(CGCGCGCGCG)^2; marker C: 12mer hairpin RNA (CGCGAAUUCGCG).

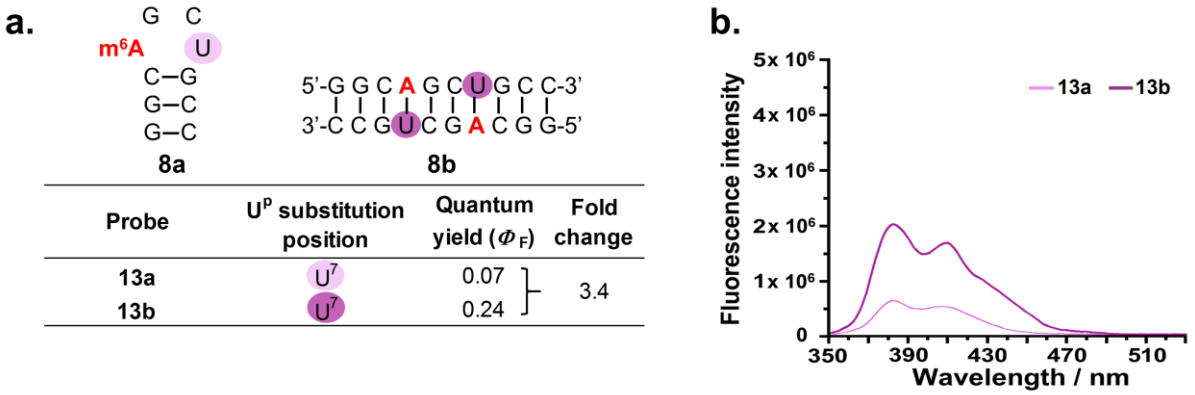

Probe	U^p substitution position	Quantum yield (Φ_F)	Fold change
13a	U^7	0.07	3.4
13b	U^7	0.24	

Fig. S9. Effects of U^p substitution position on fluorescence light-up response. (a) Uridine residues at U^7 position of probes **8a** and **8b** (colour coded) were replaced with the fluorescence nucleotide U^p to generate probes **13a** and **13b**, respectively (b) The fluorescence emission spectra of the U^p-labelled probes were recorded at an excitation wavelength of 340 nm at 5 µM strand concentration under physiologically-relevant conditions (10 mM sodium phosphate buffer containing 150 mM NaCl, pH 7.4, 37 °C). Two pyrene emission peaks at λ_{em} ~385 nm and ~410 nm were observed.

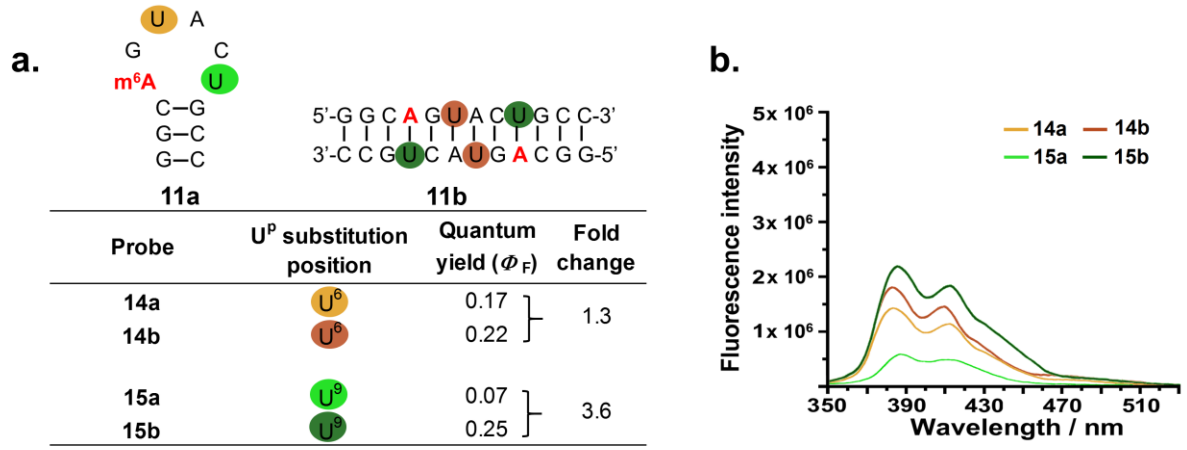

Probe	U^p substitution position	Quantum yield (Φ_F)	Fold change
14a	U^6	0.17	1.3
14b	U^6	0.22	
15a	U^9	0.07	3.6
15b	U^9	0.25	

Fig. S10. Effects of U^p substitution position on fluorescence light-up response. (a) Uridine residues at U^6 and U^9 positions of probes **11a** and **11b** (colour coded) were systematically replaced with the fluorescence nucleotide U^p. (b) The fluorescence emission spectra of the resulting probes were recorded at an excitation wavelength of 340 nm at 5 μM strand concentration under physiologically-relevant conditions (10 mM sodium phosphate buffer containing 150 mM NaCl, pH 7.4, 37 °C). Two pyrene emission peaks at λ_{em} ~385 nm and ~410 nm were observed. The pyrene fluorescence was poorly quenched at the U^6 position (**14a**), presumably due to an adjacent adenine residue which is known to be a poor quencher of pyrene. This resulted in significantly reduced fluorescence light-up response ($\Delta\Phi_F = 1.3$) compared with all other probes investigated.

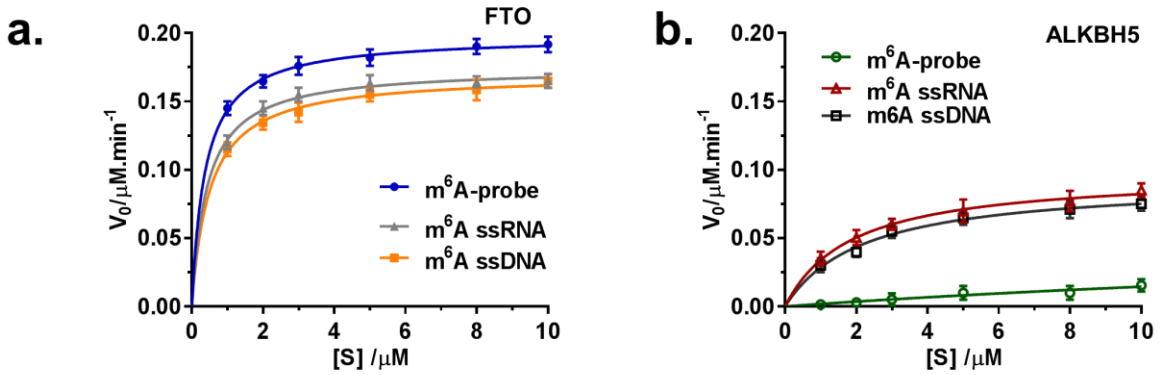

Fig. S11. Steady-state kinetics analyses of the demethylation of m^{6}A-probe, ssRNA and ssDNA substrates containing the GG(m^{6}A)CU consensus motif by m^{6}A demethylases. The K_m and k_{cat} values of (a) FTO and (b) ALKBH5 were determined by keeping a constant enzyme concentration of 0.5 μM and varying the substrate concentrations (1, 2, 3, 5, 8 and 10 μM). All reactions were performed at 4 ºC in triplicate and were adjusted to ensure that less than 20% of the substrate was consumed. Errors represent S.D. of three replicates. The m^{6}A-probe is a reasonably good substrate for FTO and could be demethylated with similar efficiency as ssRNA and ssDNA substrates. On the contrary, the m^{6}A-probe is a poor substrate for ALKBH5.

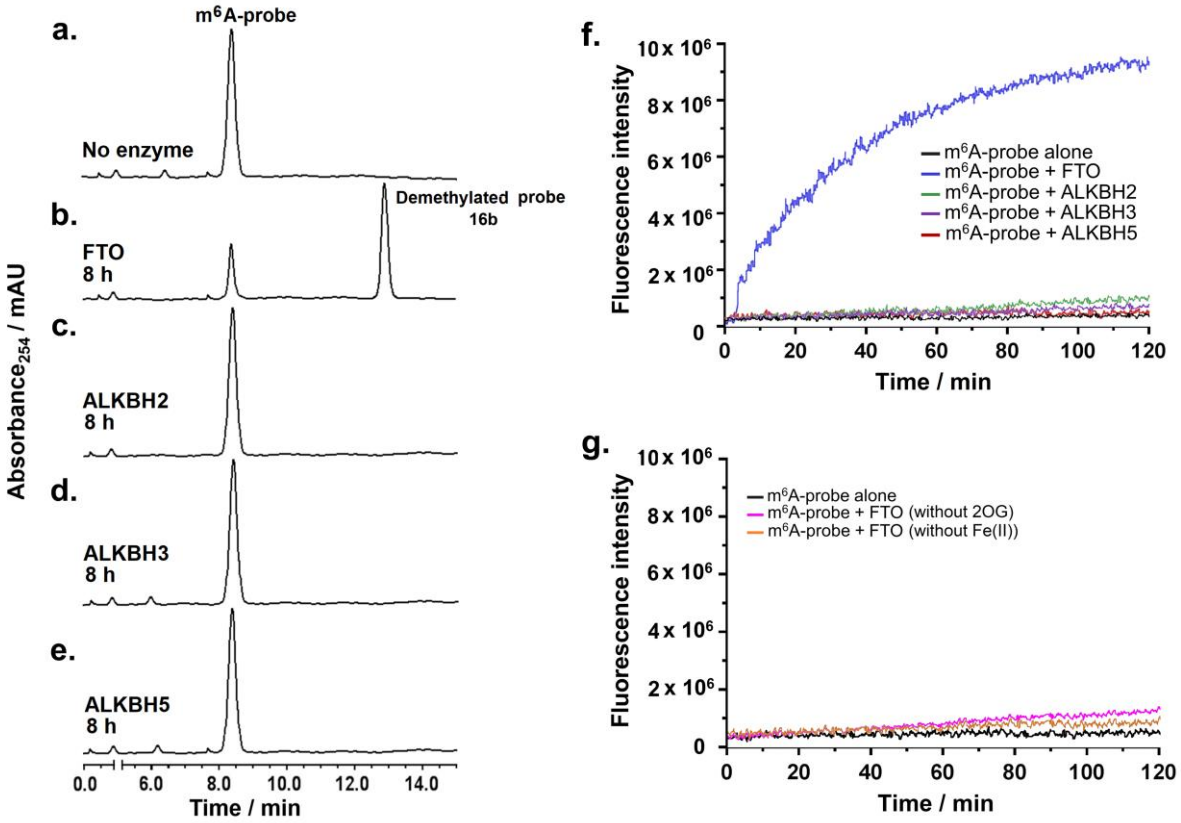

Fig. S12. HPLC-based analysis of m^{6}A-probe demethylation by AlkB demethylases. Reaction consisted of the enzyme (2 µM), m^{6}A-probe (substrate; 10 µM), 2-oxoglutarate (cosubstrate; 150 µM), $(NH_4)_2Fe(SO_4)_2 \cdot 6H_2O$ (cofactor; 150 µM), and L-ascorbate (2 mM) in 50 mM HEPES buffer, pH 7.4, 37°C. Representative HPLC traces of reaction mixtures (a) in the absence of enzyme (control), and after treatment with (b) FTO, (c) ALKBH2, (d) ALKBH3, and (e) ALKBH5; the assignment of HPLC peaks was made by comparison with known standards. The m^{6}A-probe substrate is highly selectivity for FTO over other AlkB demethylases investigated, as demonstrated by the lack of product formation with ALKBH2, ALKBH3 and ALKBH5, even after prolonged (8 hours) incubation. Consistent with demethylation-induced conformational change, the demethylated product **18b** (Rt = 12.7 min; duplex) eluted with considerably longer retention time than the m^{6}A-probe (Rt = 8.4 min; hairpin). Hence, the methylation-switchable probe approach could also facilitate the analysis of demethylase activity by HPLC-based methods. (f) Time-course fluorescence responses of m^{6}A-probe (10 µM) in the absence and in the presence of FTO (0.5 µM), ALKBH2 (2 µM), ALKBH3 (2 µM), and ALKBH5 (2 µM) showed that probe fluorescence is activated solely by FTO and not by other FTO subfamily members. Fluorescence was measured using λ_{ex} 340 nm; λ_{em} 410 nm. (g) Experiments lacking FTO or any of the key assay components *i.e.* 2OG (cosubstrate) or Fe(II) (cofactor) did not result in any fluorescence increase, suggesting that fluorescence response was dependent on FTO demethylase activity.

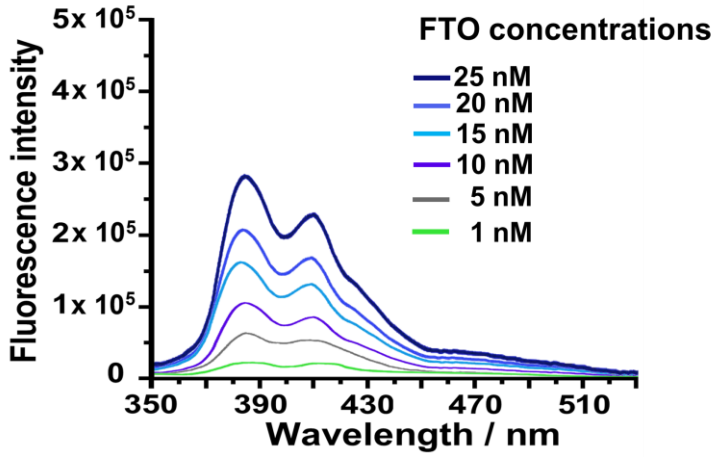

Fig. S13. Enzyme titration studies. The m^6A-probe (10 µM) was incubated with various concentrations of FTO (ranging from 1 nM to 25 nM) in the presence of $(NH_4)_2Fe(SO_4)_2 \cdot 6H_2O$ (cofactor; 10 µM), 2OG (cosubstrate; 10 µM) and L-ascorbate (200 µM) under physiologically-relevant conditions (50 mM HEPES buffer, pH 7.4). The fluorescence (λ_{ex} 340 nm) of the reaction mixture was measured after 30 min incubation at 37 °C. The fluorescence intensity is proportional to enzyme concentrations. Although m^6A demethylase activity could be detected at FTO concentrations of 5 nM and 1 nM, there is significant deviation in fluorescence signal between assays at these FTO concentrations. Fluorescence signal could only be reliably and reproducibly detected at a lowest FTO concentration of 10 nM.

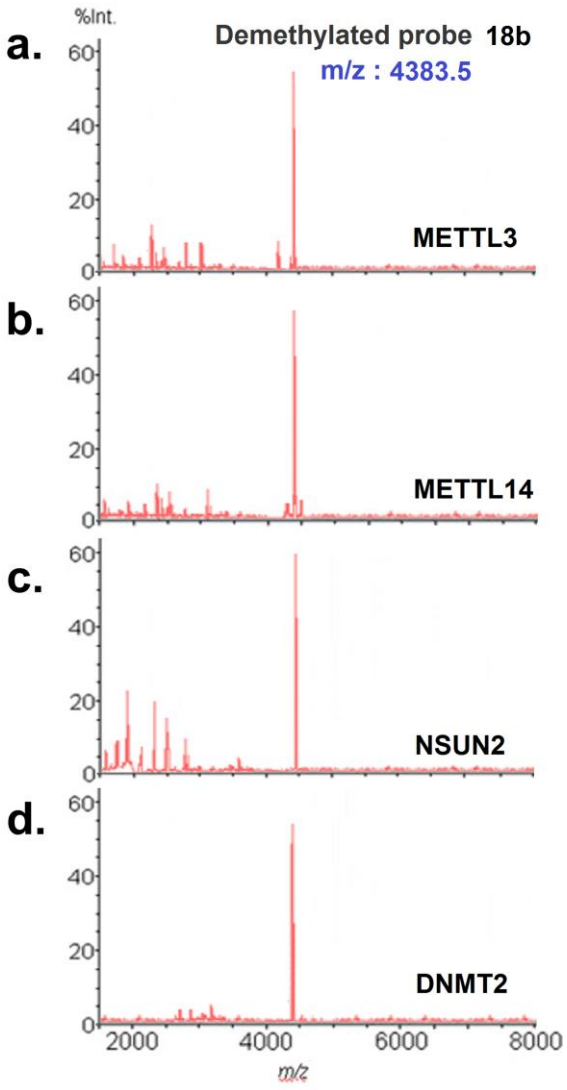

Fig. S14. Methylation analysis of the demethylated probe **18b** using a MALDI-TOF MS based assay. The demethylated probe was evaluated against two m^6A methyltransferases (a) METTL3, and (b) METTL14, and two m^5C methyltransferases (c) NSUN2, and (d) DNMT2. The enzymes (2 µM) were incubated with the demethylated probe (10 µM) in the presence of *S*-adenosyl methionine (SAM; 10 µM) in 20 mM Tris buffer (pH 7.5) containing DTT (1 mM), 0.01% Triton X-100, and 40 U of RNaseOUT/100 µL buffer. (for details of assay, see Methods). In all cases, there was no formation of methylated product, even after prolonged incubation (8 h) at 25 °C.

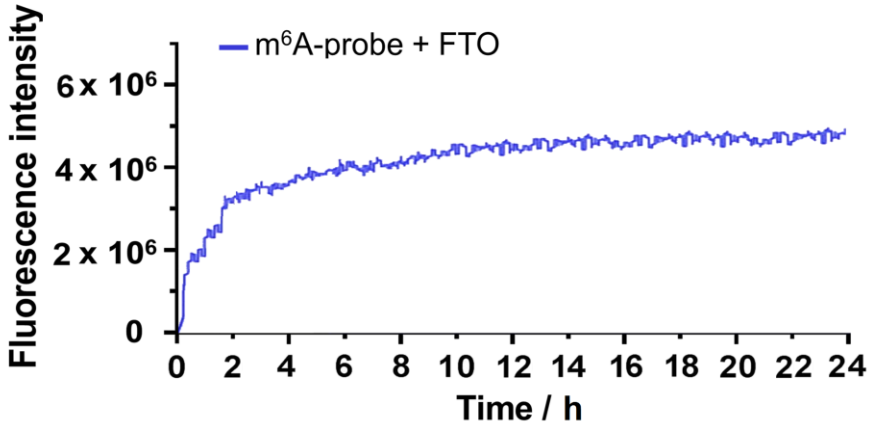

Fig. S15. Time course fluorescence analysis of the m^6A-probe in HepG2 cell lysate. The m^6A-probe (10 μM) was incubated with HepG2 cell lysate at 37 °C and the emergence of demethylated probe product was indicated by an increase in fluorescence at 410 nm (λ_{ex} 340 nm). The probe exhibited a rapid fluorescence light-up response. Maximum signal was reached in approximately 2 h, giving a ~10-fold increase in fluorescence intensity. The demethylated probe that was generated remained strongly emissive for at least 24 h, with no obvious decline in signal, suggesting that the probe has good photostability and is highly stable in cell lysate.

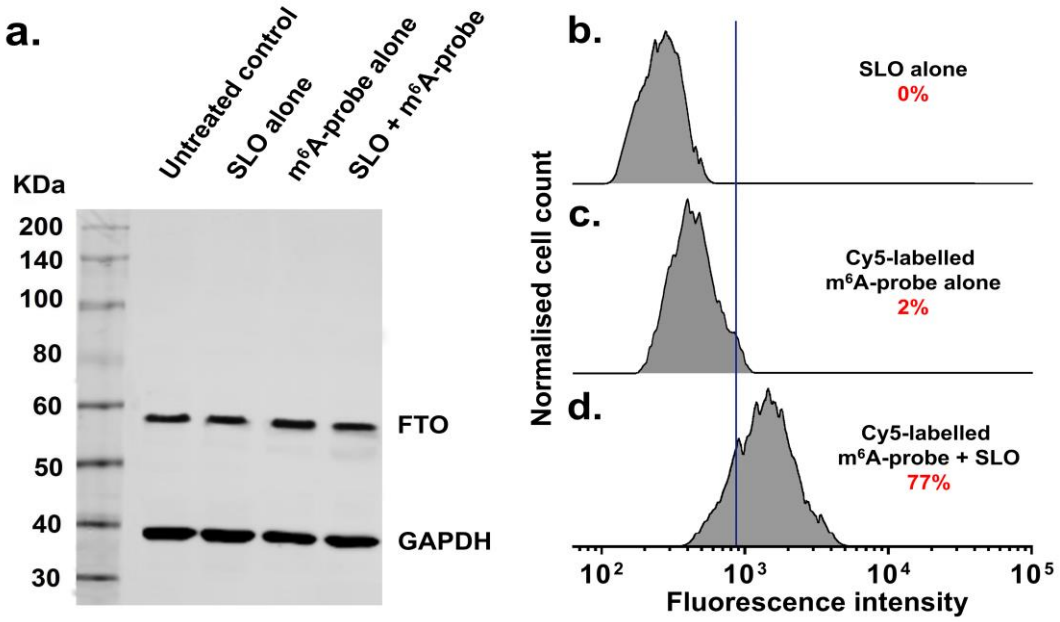

Fig. S16. The streptolysin-*O* (SLO) permeabilisation method and m^{6}A-probe do not affect cellular FTO expression. (a) Western blot analysis was performed 24 h post-SLO permeabilisation treatment (for details of SLO permeabilisation procedure, see Supporting Information). There was no significant change in FTO expression levels in the absence and presence of SLO treatment (compare lanes 1 and 2), and the uptake of m^{6}A-probe into cells also does not appear to affect FTO expression (compare lanes 2-4). A set of representative flow cytometry profiles for HepG2 cells treated with (b) SLO alone, (c) 10 μM Cy5-labelled m^{6}A-probe (in which Cy5 dye was attached to the 3'-end of m^{6}A-probe), or (d) a combination of 10 μM Cy5-labelled m^{6}A-probe and SLO. A Cy5-labelled m^{6}A-probe was used as the m^{6}A-probe itself is inherently quenched and requires fluorescence activation by FTO. Flow cytometry analysis was performed 24 h post-transfection (λ_{ex} 561 nm; λ_{ex} 661/20 nm). The Cy5-labelled probe could be effectively delivered into HepG2 cells, with a transfection efficiency of ~77% relative to control (cells treated with SLO alone); incubation with the probe alone without SLO treatment gave very poor uptake of ~2%. The SLO permeabilisation is an effective method for m^{6}A-probe delivery.

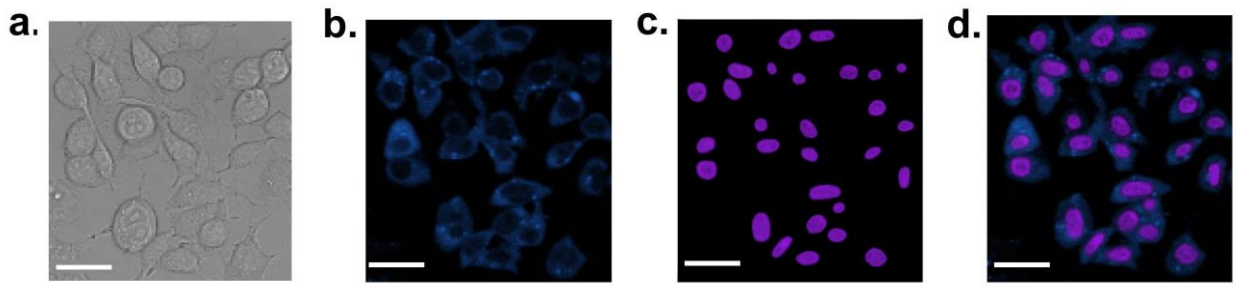

Fig. S17. The m^6A-probe appears to accumulate in the cytoplasm, with little or no detectable signal in the nucleus. Correlated (a) bright field, and (b) fluorescent images of HepG2 cells after 1 h treatment with m^6A-probe (10 μM) and (c) nuclear staining with DRAQ5. (d) Superimposition of images (b) and (c) confirmed the localisation of the probe to the cytoplasm. DRAQ5 was employed as the nuclear dye because it absorbs/emits in the far-red region (λ_{ex} 647 nm; λ_{em} 681 nm) away from m^6A-probe exicitation/emission wavelengths. Scale bar, 50 μm.

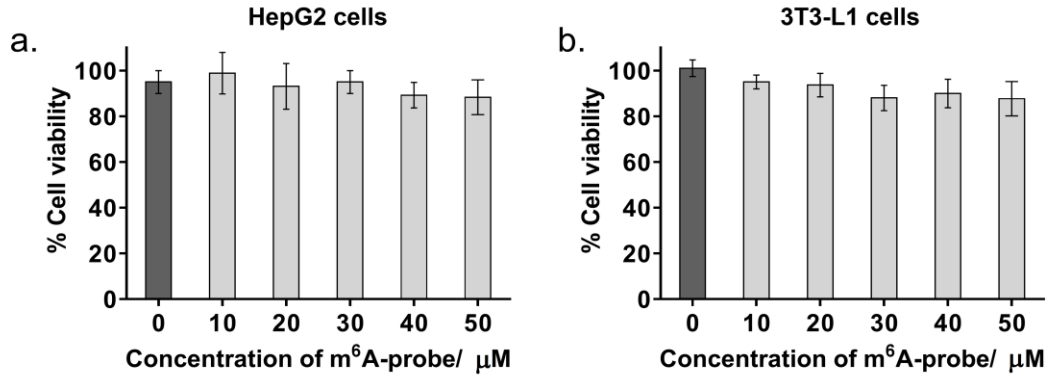

Fig. S18. MTT cytotoxicity assay demonstrated that the m^6A-probe is well-tolerated by (a) HepG2 and (b) 3T3-L1 cells, with more than 80% of the cells remaining viable after treatment with 50 μM probe for 24 h, which is within the duration of our cell-based experiments. Data are expressed as mean ± SD of three biological replicates.

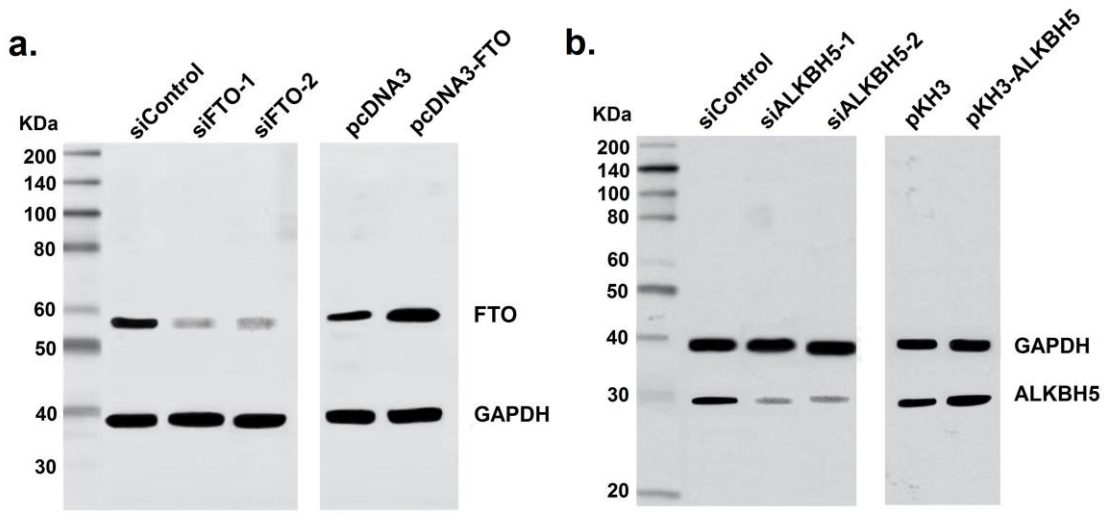

Fig. S19. Representative Western blot showing successful knockdown and overexpression of (a) FTO and (b) ALKBH5 in HepG2 cells. The siFTO and siALKBH5 concentration used was 5 nM.

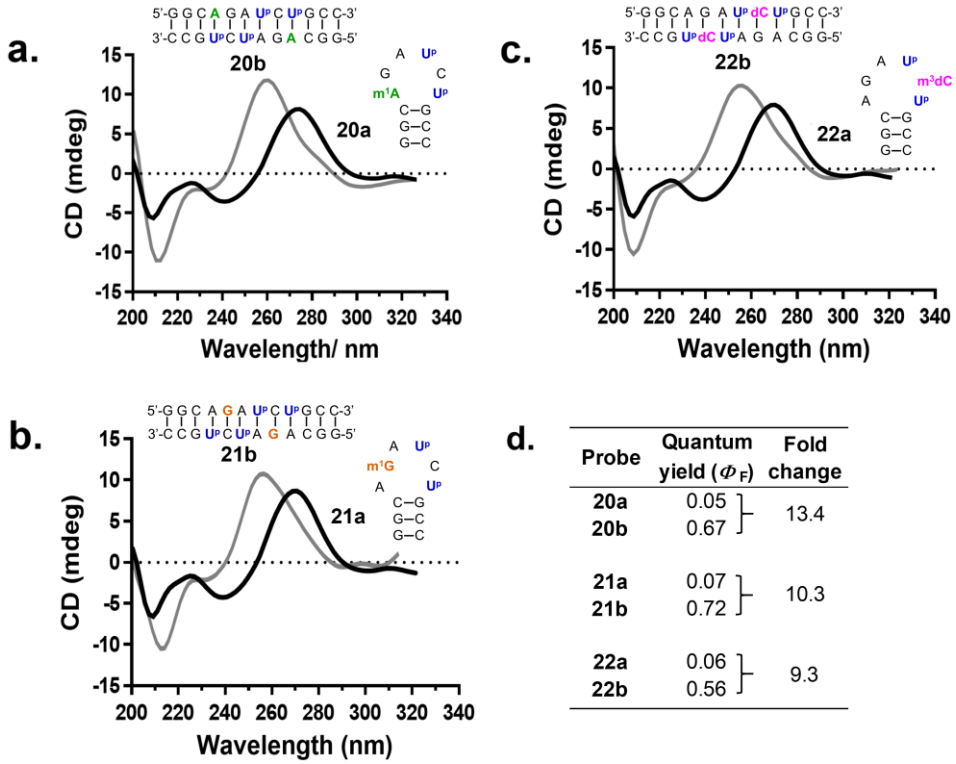

Probe	Quantum yield (Φ_F)	Fold change
20a	0.05	13.4
20b	0.67	
21a	0.07	10.3
21b	0.72	
22a	0.06	9.3
22b	0.56	

Fig. S20. Application of m^6A-probe strategy for the construction of fluorescence switchable-probes containing other physiologically-relevant base modifications, namely (a) m^1A, (b) m^1G, and (c) m^3dC. The removal of these modified bases triggered a similar hairpin-duplex conversion, as determined by CD analyses (at 5 μM strand concentration). (d) In all cases, a change in probe conformation was accompanied with a significant fluorescence light-up response ($\Delta\Phi_F > 9$). The fluorescence quantum yields (λ_{ex} 340 nm) were determined at 5 μM strand concentration under physiologically-relevant conditions (10 mM sodium phosphate buffer containing 150 mM NaCl, pH 7.4, 37 °C).

Materials and Methods

Synthesis and purification of 2'-*O*-methyl RNA probes

All oligonucleotide probes used in this study were synthesised on an Applied Biosystem 394 DNA/RNA synthesizer using standard β-cyanoethyl phosphoramidite chemistry. All synthesiser reagents and 2'-*O*-methyl phosphoramidites were purchased from Glen Research. 2'-*O*-(1-pyrenylmethyl)uridine phosphoramidite was synthesised according to literature procedure.[1] The oligonucleotides were synthesised on a CPG solid support using a standard 1 μmole phosphoramidite cycle of acid-catalysed detritylation, coupling, capping, and iodine oxidation. Coupling of 2'-*O*-(1-pyrenylmethyl)uridine and other modified monomers (e.g. m^6A, m^1A, m^3T and $m_2{}^6A$) was achieved *via* coupling reagent 5-(ethylthio)-1*H*-tetrazole using an extended coupling time of 10 min. Cleavage of the oligonucleotides from the solid support was performed by treatment with an anhydrous solution of 2 M ammonia in MeOH for 60 h at room temperature. The crude product was then lyophilised and purified by reverse-phase HPLC using the Waters XBridge OST C18 column (2.5 micron, 10 mm × 50 mm). HPLC solvents used were: solvent A (100 mM triethylammonium acetate buffer, pH 6.5 with 5% acetonitrile) and solvent B (100 mM triethylammonium acetate buffer, pH 6.5 with 15% acetonitrile) with a flow rate of 5 mL/ min. All purified oligonucleotides were characterized by MALDI-MS and capillary gel electrophoresis, and were found to be at least 95% pure. The MALDI-MS data for all probes investigated in this study are summarised in Tables S1 and S2.

Preparation of oligonucleotide probe samples:

The lyophilised oligonucleotides were reconstituted in 10 mM sodium phosphate buffer (pH 7.4) solution containing 150 mM NaCl. Their concentrations were determined by UV absorbance at 260 nm (A_{260}) using a NanoDrop ND-1000 UV-Visible Spectrophotometer. Extinction coefficients were calculated using the nearest neighbour approximation; the extinction coefficients of oligonucleotides containing methylated bases were assumed to be the same as those containing unmodified bases. The extinction coefficients of oligonucleotides containing U^p was measured using the extinction coefficients for pyrene at 340 nm ($\varepsilon_{340} = 4.7 \times 10^4\ M^{-1}cm^{-1}$). For oligonucleotides that contain two U^p (e.g. m^6A-probe) the sum of extinction coefficients for two pyrenes at 340 nm ($\varepsilon_{340} = 9.4 \times 10^4\ M^{-1}cm^{-1}$) were used.

FTO inhibitor synthesis

The FTO inhibitors (24PDCA, Rhein, IOX3 and isonicotinic acid) investigated in this study were purchased from Sigma-Aldrich. LipotF and ethyl LipotF was synthesised as previously described by us.[2] The ^{1}H NMR, ^{13}C NMR and MS data are consistent with the published data. All inhibitors were found to be at least 95% pure.

Human FTO expression and purification

Full length human FTO was expressed and purified as previously reported, with modifications.[2,3] Full length human FTO was sub-cloned into pNIC28-Bsa4 to generate a His_6-tagged FTO_{1-505} construct, which was transformed into *E. coli* BL21 (DE3) Rosetta cells. The transformed cells were grown at 37 °C and 200 rpm until an OD_{600} of 0.6 was reached. FTO expression was then induced with 0.5 mM isopropyl β-$_D$-1-thiogalactopyranoside (IPTG, Gold Biotechnology). Cell growth was continued at 16 °C for 16 h, after which the cells were harvested by centrifugation and the resulting cell pellet was stored at -80 °C. The frozen cell pellets were thawed and re-suspended to homogeneity in 25 mM Tris buffer (pH 7.5) containing 500 mM NaCl, 40 mM imidazole and 5 mM β-mercaptoethanol (β-ME). The cells were then disrupted by sonication on ice, and the cell lysate centrifuged and filtered. FTO was then purified from the resulting supernatant using Ni affinity chromatography (GE healthcare). Further purification of FTO was achieved by gel filtration using a HiLoad superdex 200 26/60 (GE healthcare) in a 25 mM Tris buffer (pH 7.5) containing 100 mM NaCl, 5% (v/v) glycerol and 5 mM β-ME.

Human ALKBH2 expression and purification

Human ALKBH2 was expressed and purified as previously reported, with modifications.[2,3] A His_6-tagged $ALKBH2_{56-258}$ construct in pET28b was transformed into *E. coli* BL21 (DE3) Rosetta cells. The transformed cells were grown at 37 °C and 200 rpm to an OD_{600} of 0.6. ALKBH2 expression was induced by addition of 0.5 mM IPTG (Gold Biotechnology). Growth was continued at 37 °C for 4 h, after which the cells were harvested by centrifugation. The resulting cell pellet was stored at -80 °C. Cell pellets were resuspended to homogeneity in 50 mM Sodium Phosphate buffer, pH 8.0, containing 300 mM NaCl, 10% (v/v) glycerol and 5 mM β-ME. The cells were then disrupted by sonication on ice, and the cell lysate centrifuged and filtered. ALKBH2 was purified from the crude cell lysate by Ni affinity chromatography (GE healthcare), with elution achieved by application of gradient to 500 mM imidazole. This was followed by anion chromatography using a 5 mL HiTrap Q HP column (GE healthcare),

with elution achieved by application of gradient to 1 M NaCl. Further purification was achieved by gel filtration using a HiLoad superdex 75 26/60 (GE healthcare) in a buffer of 10 mM Tris, pH 8.0, containing 100 mM NaCl and 5 mM β-ME. $ALKBH2_{56-258}$ has previously been shown to be catalytically active.[4]

Human ALKBH3 expression and purification

Full length human ALKBH3 was expressed and purified as previously reported, with modifications.[2,3] Full length human ALKBH3 was sub-cloned into pET28a to generate a His_6-tagged $ALKBH3_{1-286}$ construct, which was transformed into *E. coli* BL21 (DE3) Rosetta cells. The transformed cells were grown at 37 °C and 200 rpm until an OD_{600} of 0.6 was reached. ALKBH3 expression was then induced by addition of 0.5 mM isopropyl β-D-1-thiogalactopyranoside (IPTG, Gold Biotechnology). Cell growth was continued at 37 °C for 4 h, after which the cells were harvested by centrifugation and the resulting cell pellet was stored at -80 °C. The frozen cell pellets were thawed and re-suspended to homogeneity in 50 mM Sodium Phosphate, pH 8.0, 300 mM NaCl, 10 mM imidazole and 5 mM β-ME. The cells were then disrupted by sonication on ice, and the cell lysate centrifuged and filtered. ALKBH3 was then purified from the resulting supernatant using Ni affinity chromatography (GE healthcare). with elution achieved by application of gradient to 500 mM imidazole. Further purification was achieved by gel filtration using a HiLoad superdex 75 16/60 (GE healthcare) in a buffer of 25 mM Sodium Phosphate buffer, pH 8.0 containing 150 mM NaCl, 5% (v/v) glycerol and 5 mM β-ME.

Human ALKBH5 expression and purification

Human ALKBH5 (encompassing residues 66-292) was expressed and purified as previously reported, with modifications.[2,3] A His_6-tagged $ALKBH5_{66-292}$ construct in pNIC28-Bsa4a was transformed into *E. coli* BL21 (DE3) Rosetta cells. The transformed cells were grown at 37 ^{o}C and 200 rpm to an OD_{600} of 0.6. Protein expression was induced by addition of 0.5 mM IPTG (Gold Biotechnology). Growth was continued at 16 ^{o}C for 16 h, after which the cells were harvested by centrifugation. The resulting cell pellet was stored at -80 ^{o}C. Cell pellets were resuspended to homogeneity in 20 mM Tris, pH 8.0, 500 mM NaCl, 40 mM imidazole, pH 8.0 and 5 mM β-ME. The cells were then disrupted by sonication on ice, and the cell lysate centrifuged and filtered. ALKBH5 was purified from the crude cell lysate by Ni affinity chromatography (GE healthcare), with elution achieved by application of gradient to 500 mM imidazole. This was followed by anion chromatography using a 5 mL HiTrap Q HP column

(GE healthcare), with elution achieved by application of gradient to 1 M NaCl. Further purification was achieved by gel filtration using a HiLoad superdex 75 26/60 (GE healthcare) in a buffer of 20 mM Tris, pH 8.0, 100 mM NaCl and 5 mM β-ME. ALKBH5$_{66-292}$ has previously been shown to be catalytically active.[4]

Human METTL3 expression and purification

Full length human METTL3 (encompassing residues 1-580) was expressed and purified as previously reported, with modifications.[5] A His$_6$-tagged METTL3$_{-1-580}$ construct in pETDuet was transformed into *E. coli* BL21 (DE3) pLysS cells. The transformed cells were grown at 37 ^{o}C and 200 rpm to an OD$_{600}$ of 0.6. Protein expression was induced by addition of 0.5 mM IPTG (Gold Biotechnology). Growth was continued at 16 ^{o}C for 16 h, after which the cells were harvested by centrifugation and sonicated in lysis buffer (50 mM Bis-Tris pH 7.0 containing 1 M NaCl, 1 mM DTT, and protease inhibitors). METTL3 was purified from the crude cell lysate by Ni affinity chromatography (GE healthcare), with elution achieved by application of gradient to 500 mM imidazole. This was followed by anion chromatography using a 5 mL HiTrap Q HP column (GE healthcare), with elution achieved by application of gradient to 1 M NaCl. Further purification was achieved by gel filtration using a HiLoad superdex 200 26/60 (GE healthcare) in a 50 mM Bis-Tris buffer (pH 7.0) containing 100 mM NaCl, 5% (v/v) glycerol and 5 mM β-ME.

Human METTL14 expression and purification

Human METTL14 (encompassing residues 1-399) was expressed and purified as previously reported, with modifications.[5] A His$_6$-tagged METTL14$_{-1-399}$ construct in pETDuet was transformed into *E. coli* BL21 (DE3) pLysS cells. The transformed cells were grown at 37 ^{o}C and 200 rpm to an OD$_{600}$ of 0.6. Protein expression was induced by addition of 0.5 mM IPTG (Gold Biotechnology). Growth was continued at 16 ^{o}C for 16 h, after which the cells were harvested by centrifugation and sonicated in lysis buffer (50 mM Bis-Tris pH 7.0 containing 1 M NaCl, 1 mM DTT, and protease inhibitors). METTL14 was purified from the crude cell lysate by Ni affinity chromatography (GE healthcare), with elution achieved by application of gradient to 500 mM imidazole. This was followed by anion chromatography using a 5 mL HiTrap Q HP column (GE healthcare), with elution achieved by application of gradient to 1 M NaCl. Further purification was achieved by gel filtration using a HiLoad superdex 200 26/60 (GE healthcare) in a 50 mM Bis-Tris buffer (pH 7.0) containing 100 mM NaCl, 5% (v/v) glycerol and 5 mM β-ME.

NSUN2 and DNMT2 proteins

Full length human NSUN2 protein (encompassing residues 1-767) was purchased from Origene Technologies, Inc. USA.

Full length human DNMT2 protein (encompassing residues 1-391 containing *N*-terminal His tag) was purchased from abcam plc. UK.

UV-based melting analysis

The melting of each RNA probes was performed on a Cary 3000 UV-Visible Spectrophotometer (Varian) at a total strand concentration of 5 μM (unless stated otherwise) in 10 mM sodium phosphate buffer, pH 7.4 and 150 mM NaCl. Absorbance versus temperature profiles were recorded at 260 nm. The samples were first denatured by heating to 95 °C at 10 °C/min, followed by slow cooling to 25 °C at 0.4 °C/min to ensure a complete annealing of the strands. The melting transitions were then monitored by heating to 95 °C at 0.4 °C/min. To increase the accuracy of measurements, the sixth position was used to record the temperature data points by placing a temperature probe directly in the cuvette. Up to six melting transitions were measured for each oligonucleotide and the average T_m values were calculated using Varian Cary Software. Each probe was measured at seven different concentrations (1, 2, 5, 10, 20, 30 and 50 μM), and a total of six melting transitions were measured for each concentration. Melting transitions were generally found to be reproducible for all probes.

Analysis of thermodynamic data from UV melting experiments

The thermodynamic data for bimolecular duplex structures *e.g* demethylated probe **16b** was analysed as previously described, with modifications.[6] The melting transitions for duplex structures were assumed to proceed in a two-state manner, and to obey the van't Hoff's equation below.

$$\frac{1}{T_m} = \frac{R}{\Delta_b H^\circ} \ln c_T + \frac{\Delta_b S^\circ}{\Delta_b H^\circ}$$

A plot of $1/T_m$ versus ln(total strand concentration) gives a straight line, where the slope is $R/\Delta H°$ and the y-intercept is $\Delta S°/\Delta H°$. Data were fitted using linear least-squares minimisation using GraphPad Prism. The free Gibbs energy ($\Delta G°$) were calculated at 37 °C (310.15 K) using the following equation.

$$\Delta_b G^\circ = \Delta_b H^\circ - T\Delta_b S^\circ$$

The thermodynamic data for monomolecular hairpin structures *e.g* m^6A-probe, m^1A-probe, m^3T-probe, and $m^6{}_2$A-probe was analysed as previously described, with modifications.[7] The experimental fluorescence versus temperature curves were first converted into a fraction of strands remaining hybridized (α) versus temperature curves. This were then fitted to a two-state transition model, where Δ*H*° and Δ*S*° values may be obtained.

Circular dichroism (CD) spectroscopy of the conformational probes

The CD spectra for the probes were obtained with a JASCO J-810 spectropolarimeter. The measurements were carried out with 5 μM probes in a 10 mM sodium phosphate buffer (pH 7.4) containing 150 mM NaCl at 25 °C. The concentrations were determined by UV absorbance at 260 nm (A_{260}) using a NanoDrop ND-1000 UV-Visible Spectrophotometer. The probe solutions were first heated to 90 °C for 5 min, and re-annealed by slow cooling to 4 °C at a rate of 1 °C/min. CD spectra were then recorded in quartz cuvettes (path length 1 mm, 400 μL) from 200 nm to 350 nm at 4 °C using a 10 nm/min scan speed, a spectral band width of 1 nm and a time constant of 4 s. All the spectra were subtracted with the buffer blank and smoothed using the Savitsky-Golay algorithm (polynomial order 10).

Non-denaturing polyacrylamide gel electrophoresis (PAGE) analysis

Annealed oligonucleotides were loaded to 20% native polyacrylamide gel and electrophoresis was performed at 4 °C in Tris/Borate/EDTA (TBE) running buffer (90 mM Tris, pH 8.3, 90 mM boric acid and 5 mM EDTA). The gel were stained with SYBR® Gold Nucleic Acid Gel Stain and visualized by Gel Dock XR + (Bio-Rad) and Image Lab 4.0 software (Bio-Rad).

Fluorescence analysis of the probes

Fluorescence was performed in a quartz cuvette using a fluorescence spectrophotometer. The fluorescence emission spectra (λ_{em} = 350-530 nm) of the probes were recorded at 5 μM strand concentration in 10 mM sodium phosphate buffer containing 150 mM NaCl, pH 7.4, 37°C. Background fluorescence spectra were acquired after the probe has been incubated for 5 min at 37 °C. The time course of fluorescence activation was recorded immediately after the addition of enzymes (0.5 μM). An average of five scans was recorded using an excitation slit width of 5.0 nm, emission slit width of 2.5 nm, and a scan speed of 600 nm/min.

Determination of fluorescence quantum yields of the probes

The fluorescence quantum yields (Φ_F) of the probes were calculated using the equation below, as previously described.[8,9] The reported quantum yields are an average of three measurements within ±10%.

$$\Phi_F(\text{probe}) = \Phi_F\,(\text{PBA}) \times \frac{A(\text{probe})}{A_{340}(\text{probe})} \times \frac{1}{\alpha(\text{PBA})} \times \frac{\eta(H_2O)^2}{\eta(\text{MeOH})^2}$$

Where Φ_F(PBA) is the cross-calibrated value for the fluorescence quantum emission yield of pyrenebutanoic acid (PBA) in MeOH. Under our experimental conditions, the fluorescence quantum yield of PBA was determined to be 0.061, which is highly consistent with the reported value of 0.065.[8,9]

A(probe) is the area of the fluorescence emission spectra of the sample from 350 to 530 nm

A_{340}(probe) is the absorbance of the sample at λ_{ex} 340 nm

α(PBA) is the slope of the fluorescence emission versus A_{340}(probe) calibration curve for PBA

η(H_2O) and η(MeOH) are the refractive indexes of water (1.3328) and methanol (1.3288), respectively.

High-throughput m^{6}A-probe assay (*in vitro*)

The assay was performed in triplicate in a final reaction volume of 25 µL in a Corning Costar 384-well flat bottom black plate. Samples were dispensed into the well using an Eppendorf Repeater Xstream pipette. Reaction consisted of FTO (50 nM), m^{6}A-probe (substrate; 10 µM), inhibitor (varying concentrations), 2-oxoglutarate (10 µM), $(NH_4)_2Fe(SO_4)_2 \cdot 6H_2O$ (10 µM), and L-ascorbate (200 µM) in 50 mM HEPES buffer, pH 7.4, 37 ºC. The fluorescence emission was measured with a Tecan ultra microplate reader using an excitation wavelength of 340 nm and an emission wavelength of 410 nm. Fluorescence was acquired for the first 30 min.

For IC_{50} determination:

Eight different concentrations of inhibitors were used (0, 1, 3, 10, 30, 100, 300, 1000 µM). The IC_{50s} were then calculated from the variation in fluorescence at different inhibitor concentrations, using nonlinear regression, with normalized dose-response fit on GraphPad Prism 6.0™. The assay was performed in triplicate for each inhibitor concentration.

For the determination of Z' factor:

The Z' factor for our m^{6}A-probe assay was calculated using the method described by Zhang *et al.*[10] A total of 40 independent assays were run with either LipotF (positive control) or DMSO (negative control). The Z' factor was then calculated using the equation below.[10]

$$Z'factor = 1 - \frac{3(\sigma p + \sigma n)}{\mu_p - \mu_n}$$

Where μ_p and μ_n are the means of the positive (p) and negative (n) controls

σ_p and σ_n are the standard deviations of the positive (p) and negative (n) controls.

The following guideline was used to interpret the Z' factor.

A Z' factor between 0.5 and 1.0 indicates an excellent assay.

A Z' factor between 0 and 0.5 indicates a marginal assay.

A Z' factor < 0 indicates too much signal overlap between the positive and negative controls for the assay to be useful.

HPLC-based demethylase assay

The assay was modified from previously reported method.[2,3] The assay was performed in triplicate in a final reaction volume of 25 µL. Reaction consisted of 1 µM enzyme, 10 µM m^{6}A substrate (either m^{6}A-probe or m^{6}A-ssRNA r(5'-GCGG-**m^{6}A**-CUCCAGAUG-3') or m^{6}A-ssDNA d(5'-GCGG-**m^{6}A**-CTCCAGATG-3'), 2-oxoglutarate (150 µM), $(NH_4)_2Fe(SO_4)_2 \cdot 6H_2O$ (150 µM), and L-ascorbate (2 mM) in 50 mM HEPES buffer, pH 7.4. The reaction was incubated at 37 ºC for the specified time points, before analysis on a bio-inert HPLC system. The m^{6}A substrate and the corresponding demethylated product were separated using a Dionex DNAPac PA200 anion-exchange column (8 µm, 4 mm × 25 mm) with a gradient of 98% solvent A (50 mM sodium citrate buffer, pH 5.3) to 35% solvent B (50 mM sodium citrate buffer, pH 5.3 with 1.0 M sodium chloride) over 10 min, at a flow rate of 1 mL/min at 40 °C. The UV detection wavelength was set at 266 nm. Controls without enzyme were also set up. The percentage demethylation was estimated based on the peak areas of the m^{6}A-probe relative to the control.

Steady-state kinetic analyses of the demethylation of m^{6}A-probe, m^{6}A-containing ssRNA and m^{6}A-containing ssDNA.

The substrates investigated include m^{6}A-probe or m^{6}A-ssRNA r(5'-GCGG-**m^{6}A**-CUCCAGACG-3') or m^{6}A-ssDNA d(5'-GCGG-**m^{6}A**-CdUCCAGACG-3'). The consensus 'GG(m^{6}A)CU' motif was underlined. The K_m and k_{cat} values of FTO and ALKBH5 were determined by keeping a constant enzyme concentration of 0.5 μM and varying the substrate concentrations (2.5, 5, 10, 15, 20 and 30 μM). The concentration of demethylated product at different substrate concentrations was plotted as a function of time. The initial velocity (V_0) for each substrate concentration was determined from the slope of the curve at the beginning of a reaction. The Michaelis–Menten curve was fitted using non-linear regression, and the kinetic constants (V_{max}, K_m) of the substrate was estimated using GraphPad Prism. All reactions were performed at 37 ºC in triplicate and were adjusted to ensure that less than 20% of the substrate was consumed.

Methyltransferase activity assay (with METTL3, METTL14, NSUN2 and DNMT2)

The methyltransferase activity assay was carried out in as previously described, with modifications.[11] The reaction was performed triplicate in 50 μL of reaction mixture containing the following components: m^{6}A-probe (10 μM), MTase (2 μM; either METTL3 or METTL14 or NSUN2 or DNMT2), *S*-adenosyl methionine (SAM; 10 μM) in 20 mM Tris (pH 7.5) buffer containing DTT (1 mM), 0.01% Triton X-100, and 40 U of RNaseOUT/100 μL buffer. The reaction was incubated at 25 °C for 8 h before 1:1 quenching with 20% v/v formic acid. 1 uL of the diluted assay mixture was then mixed with 1 uL of 3-hydroxpicolinic acid (3-HPA, the MALDI-TOF-MS matrix, Sigma-Aldrich) and spotted onto the MALDI-TOF-MS plate before analysis. The 3-HPA matrix was prepared by mixing 9 parts of 50 mg/mL 3-hydroxpicolinic acid in 50% MeCN/Milli-Q H_2O with 1 part of 50 mg/mL ammonium citrate in Milli-Q H_2O. The percentage inhibition was estimated based on the relative intensities of the methylated substrate and the demethylated product observed in the mass spectra.

HepG2 cell culture, siRNA knockdown and plasmid transfection.

HepG2 cells (ATCC) were cultured in Dulbecco's modified Eagle's medium (DMEM; Life Technologies) containing 4.5 g/L $_D$-glucose, L-glutamine and 10% fetal bovine serum (FBS), in a humidified incubator containing 5% CO_2 environment, as previously described.[12] Transfection was achieved by using Lipofectamine RNAiMAX (Invitrogen) for siRNA or Lipofectamine 2000 (Invitrogen) for the plasmid following the manufacturer's protocols. The

siRNAs for FTO and ALKBH5 were purchased from Integrated DNA Technologies with the sequences shown below. The construct for full length FTO was cloned into mammalian vector pcDNA3 with *N*-terminal FLAG-tag. The construct for full length ALKBH5 was cloned into mammalian vector pKH3 with *N*-terminal triple HA-tag. Both constructs were purchased from GenScript.

siFTO-1: 5'-UUAAGGUCCACUUCAUCAUCGCAGG-3'

siFTO-2: 5'-CAGGCACCUUGGAUUAUAUTT-3'

siALKBH5-1: 5'-ACAAGUACUUCUUCGGCGA-3'

siALKBH5-2: 5'-GCGCCGUCAUCAACGACUA-3'

siControl: 5'-UUCUCCGAACGUGUCACGU-3'

HepG2 whole cell lysate preparation.

HepG2 cell lysate was prepared by homogenisation in a modified RIPA lysis buffer (150 mM sodium chloride, 50 mM Tris-HCl, pH 7.4, 1 mM ethylenediamine tetraacetic acid, 1 mM phenylmethylsulfonyl flouride, 1% Triton X-100, 1% sodium deoxycholic acid, 0.1% sodium dodecylsulfate, 5 μg/mL of aprotinin, 5 μg/mL of leupeptin). Cell debris was removed by centrifugation. Total protein concentration was determined by a Bradford assay.

3T3-L1 pre-adipocyte differentiation

3T3-L1 pre-adipocytes (ATCC) were grown in DMEM containing 10% fetal bovine serum (FBS), penicillin (100 U/mL) and streptomycin (100 μg/mL) until confluence, as previously described.[13] To induce differentiation, cells that were two days' post-confluence (designated as day 0) were exposed to differentiation medium containing containing 0.5 mmol/L 3-isobutyl-1-methylxanthine (IBMX), 1 μmol/L dexamethasone, 1 μg/mL insulin, 2 μmol/L rosiglitazone and 10% FBS for 3 days. At the end of day 3, culture medium was replaced with DMEM supplemented only with 10 μg/mL insulin and 10% FBS, and replenished every other day. By day 10, at least 90% of the cells had accumulated lipid droplets and have differentiated into mature adipocytes.

To follow the dynamic changes in endogenous FTO activity and cellular m^6A levels during adipogenesis:

The m^6A-probe (10 μM) was delivered into the cells at different time points of adipogenesis (Day 0, 3, 6, 9), followed by analyses with fluorescence microscopy and flow cytometry, as described below.

Delivery of m^{6}A-probe into cells

The m^{6}A-probe was delivered into living cells using a reversible permeabilisation method with streptolysin-*O* (SLO), as previously described.[14] This method was reported to be more rapid and efficient compared with conventional transfection methods. SLO was first activated by adding 5 mM of TCEP to 2 U/mL of SLO for 30 min at 37°C. Cells that were grown in a 4-chamber well (~2 x 10^5 cells per well; 80% confluency) were incubated for 10 min with 200 μL of serum free medium containing 0.2 U/mL of activated SLO and 10 μM of m^{6}A-probe or control probe **22a**. The cells were then resealed by adding 0.5 mL of growth medium and incubated for a further 1 h at 37°C (unless otherwise specified). The cells were then washed with 1x PBS before analysis with fluorescence microscopy or flow cytometry as described below.

Fluorescence microscopy

Fluorescence images were acquired using a Nikon BioStation IM-Q live cell imaging system equipped with 20x and 63x oil immersion objective lens. The DAPI filter setting was used (*i.e.* λ_{ex} = 340-380 nm, dichroic mirror allowing passage of λ > 400 nm, and λ_{em} 435-485nm). For each fluorescence image, the corresponding transmitted light image was also acquired. Quantification of images was performed using the Biostation IM multichannel software. Fluorescence intensity was measured by only collecting average gray values for regions exhibiting fluorescence. All experiments were performed in triplicates and the mean fluorescence intensities were normalised to that of the control.

Flow cytometry

Cells that were pre-treated with m^{6}A-probe (10 μM) or control probe **22a** (10 μM; as described above) were collected by trypsinisation at 37 °C with 5% CO_2, washed with PBS media, resuspended in PBS media and then analysed using a BD LSRFortessa™ flow cytometer (BD Bioscience). Fluorescence was measured using an excitation laser of 355 nm, and a 450/50 bandpass emission filter. Acquisition was stopped when 20,000 events per sample were acquired. The fluorescence data were then analysed using BD FACS software.

Real-time fluorescence m^{6}A-probe assays in living cells

The HepG2 cells were pre-incubation with various concentrations (0 μM, 25 μM, 100 μM) of ethyl LipotF (a selective, cell permeable FTO inhibitor developed in our lab)[2] for 1 h at 37 °C These concentrations were shown to be non-toxic in various cell lines.[2] This was followed by

the delivery of either the m^6A-probe (10 μM) or control probe **22a** (10 μM) into the cells *via* the streptolysin-*O* permeabilisation method described above. Aliquots ware then taken out for flow cytometry measurements (λ_{ex} 355 nm; λ_{em} 379 nm) at the indicated time points (See Figure 6d-f). The mean fluorescence intensity of at least 20000 live cells was determined.

Western blot analysis

Cells were lysed using mammalian lysis buffer (Sigma-Aldrich), and immunoblotting was performed using standard protocol. The primary antibodies used were purchased from commercial sources: Mouse monoclonal anti-FTO (Abcam, ab92821), rabbit polyclonal anti-ALKBH5 (Sigma-Aldrich), and anti-GAPDH antibody (Cell Signalling; loading control). Membranes were washed with TBST and incubated with either horseradish peroxidase (HRP)-conjugated anti-rabbit IgG antibody (Bio-Rad) or HRP-conjugated anti-mouse IgG antibody (Bio-Rad) for 2 h at room temperature. Enhanced chemiluminescence substrates (Luminata Crescendo, EMD Millipore) were then applied, and the signals exposed to autoradiography film. The immunoblots were then quantified by densitometric analyses using ImageJ software.

RNA m^6A quantification by dot-blot analysis

Total RNA was isolated from the cells with TRIZOL reagent (Invitrogen), as previously described.[13] The mRNA was then isolated from total RNA using the Dynabeads® mRNA Purification Kit following the manufacturer's instructions. The concentration of purified mRNA was then determined with NanoDrop and the mRNA serially diluted to 50 ng/μL and 25 ng/μL using RNase-free water. For dot-blot analysis, the mRNA was first denatured by heating at 95 ºC in a heat block for 3 min, followed by immediate chilling on ice to prevent the re-formation of secondary structures of mRNA. 2 μL of the mRNA was spotted on an Amersham Hybond-N^+ membrane optimised for nucleic acid transfer (GE Healthcare) and crosslinked *via* a UV crosslinker. The membrane was then washed using wash buffer (1x PBS with 0.02% Tween-20), blocked with 5% of non-fat milk in wash buffer, and incubated with anti-m^6A antibody (1:250 dilution; 2 μg/ml; abcam) in 10 mL of antibody dilution buffer overnight at 4 °C with gentle shaking. Horseradish peroxidase (HRP)-conjugated anti-rabbit IgG secondary antibody (1:10000 dilution; 20 ng/ml) was then added and the membrane visualised by ECL Western Blotting Detection Kit (GE Healthcare). To ensure an equal amount of mRNA was spotted on the membrane, the same blot was stained with 0.02% methylene blue in 0.3 M sodium acetate (pH 5.2). The signals from the dot blot images was quantified by ImageJ and statistical analysis was based on three replicates.

References

(1) Karmakar, S.; Anderson, B. A.; Rathje, R. L.; Andersen, S.; Jensen, T. B.; Nielsen, P.; Hrdlicka, P. J. High-Affinity DNA Targeting Using Readily Accessible Mimics of N2′-Functionalized 2′-Amino-α-L-LNA. *J. Org. Chem.* **2011**, *76*, 7119-7131.

(2) Toh, J. D. W.; Sun, L.; Lau, L. Z. M.; Tan, J.; Low, J. J. A.; Tang, C. W. Q.; Cheong, E. J. Y.; Tan, M. J. H.; Chen, Y.; Hong, W.; Gao, Y.-G.; Woon, E. C. W. A Strategy Based on Nucleotide Specificity Leads to a Subfamily-Selective and Cell-Active Inhibitor of *N* 6 -Methyladenosine Demethylase FTO. *Chem. Sci.* **2015**, *6*, 112-122.

(3) Zou, S.; Toh, J. D. W.; Wong, K. H. Q.; Gao, Y.-G.; Hong, W.; Woon, E. C. Y. N 6-Methyladenosine: A Conformational Marker That Regulates the Substrate Specificity of Human Demethylases FTO and ALKBH5. *Sci. Rep.* **2016**, *6*, 25677.

(4) Yang, T.; Cheong, A.; Mai, X.; Zou, S.; Woon, E. C. Y. A Methylation-Switchable Conformational Probe for the Sensitive and Selective Detection of RNA Demethylase Activity. *Chem. Commun. (Camb).* **2016**, *52*, 6181-6184.

(5) Wang, P.; Doxtader, K. A.; Nam, Y. Structural Basis for Cooperative Function of Mettl3 and Mettl14 Methyltransferases. *Mol. Cell* **2016**, *63*, 306-317.

(6) Marky, L. A.; Breslauer, K. J. Calculating Thermodynamic Data for Transitions of Any Molecularity from Equilibrium Melting Curves. *Biopolymers* **1987**, *26*, 1601-1620.

(7) Xia, T.; Mathews, D. H.; Turner, D. H. Thermodynamics of RNA secondary structure formation. In Söll, D.; Nishimura, S. and Moore, P. (eds), *Comprehensive Natural Product Chemistry* **1999**, *8*, 21-47; Elsevier, Oxford, UK.

(8) Morris, J. V.; Mahaney, M. A.; Huber, J. R. Fluorescence Quantum Yield Determinations. 9,10-Diphenylanthracene as a Reference Standard in Different Solvents. *J. Phys. Chem.* **1976**, *80*, 969-974.

(9) Netzel, T. L.; Nafisi, K.; Headrick, J.; Eaton, B. E. Direct Observation Of Photoinduced Electron Transfer In Pyrene-Labeled Du Nucleosides and Evidence For Protonated 2'-Deoxyuridine Anion, du(H).cntdot., As a Primary Electron Transfer Product. *J. Phys. Chem.* **1995**, *99*, 17948-17955.

(10) Zhang, J. H.; Chung, T. D. Y.; Oldenburg, K. R. A Simple Statistical Parameter for Use in Evaluation and Validation of High Throughput Screening Assays. *J. Biomol. Screen.* **1999**, *4*, 67-73.

(11) Li, F.; Kennedy, S.; Hajian, T.; Gibson, E.; Seitova, A.; Xu, C.; Arrowsmith, C. H.; Vedadi, M. A Radioactivity-Based Assay for Screening Human m6A-RNA Methyltransferase,

METTL3-METTL14 Complex, and Demethylase ALKBH5. *J. Biomol. Screen.* **2016**, *21*, 290-297.

(12) Lim, A.; Zhou, J.; Sinha, R. A.; Singh, B. K.; Ghosh, S.; Lim, K. H.; Chow, P. K. H.; Woon, E. C.; Yen, P. M. Hepatic FTO Expression Is Increased in NASH and Its Silencing Attenuates Palmitic Acid-Induced Lipotoxicity. *Biochem. Biophys. Res. Commun.* **2016**, *479*, 476-481.

(13) Zhao, X.; Yang, Y.; Sun, B. F.; Shi, Y.; Yang, X.; Xiao, W.; Hao, Y. J.; Ping, X. L.; Chen, Y. S.; Wang, W. J.; Jin, K. X.; Wang, X.; Huang, C. M.; Fu, Y.; Ge, X. M.; Song, S. H.; Jeong, H. S.; Yanagisawa, H.; Niu, Y.; Jia, G. F.; Wu, W.; Tong, W. M.; Okamoto, A.; He, C.; Rendtlew, Danielsen, J. M.; Wang, X. J.; Yang, Y. G. FTO-Dependent Demethylation of N6-Methyladenosine Regulates mRNA Splicing and Is Required for Adipogenesis. *Cell Res.* **2014**, *24*, 1403-1419.

(14) Robinson, L. J.; Pang, S.; Harris, D. S.; Heuser, J.; James, D. E. Translocation of the Glucose Transporter (GLUT4) to the Cell Surface in Permeabilized 3T3-L1 Adipocytes: Effects of ATP, Insulin, and GTP gamma S and Localization of GLUT4 to Clathrin Lattices. *J. Cell Biol.* **1992**, *117*, 1181-1196.